Nondestructive Testing and Evaluation,
Vol. 22, Nos. 2–3, June–September 2007, 199–215

Qualitative and quantitative assessment of aerospace structures by pulsed thermography

C. IBARRA-CASTANEDO†, M. GENEST‡, P. SERVAIS¶, X. P. V. MALDAGUE*† and A. BENDADA†

†Computer Vision and Systems Laboratory, Laval University, Quebec City, Que., Canada G1K7P4
‡Institute for Aerospace Research (IAR), National Research Council Canada (NRC), 1200 Montreal Road, Bilding M-14, Room 130, Ottawa, ON., Canada K1A 0R6
¶Belgian Air Force, Competence Center Flying Material, Center Flying Material, Non Destructive Testing Squadron, 1130 Brussels, Belgium

Pulsed thermography (PT) is an NDT&E technique allowing the remote examination of materials and systems. PT is particularly interesting for the inspection of aerospace structures since it can be used to perform safe inspection of large structures in a fast manner and without having to remove the components from the aircraft. Pulsed thermographic data however, is contaminated by noise of many forms. Fortunately, numerous signal processing techniques are available to perform qualitative and quantitative data analysis of data. In this paper, we present three processing techniques that have shown very promising results. We provide the theoretical background and experimental details as well as some representative results that highlight the *pros* and *cons* of each technique. As it will be pointed out, an interesting approach is the combination of existing processing techniques in order to use the most attractive features from each technique while reducing the non-desirable characteristics.

Keywords: Pulsed thermography; Differential absolute contrast; Thermographic signal reconstruction; Pulsed phase thermography; Aerospace structures

AMS Subject Classification: 68U10

1. Introduction

The role of inspection and maintenance in the aerospace industry has progressively increased since the 1980s when it became clear that aircraft were exceeding their original design life and that early detection and repair were critical to avoid catastrophic events (Ducar 1999, Achenbach 2000). Composites are probably the material most widely used material in aerospace nowadays. Fibre reinforced plastics are a common type that can be made of carbon (CFRP), glass (GFRP), Kevlar®, Nomex® or other fibers embedded in an epoxy matrix to form a ply that can be combined with other plies and can be shaped to form different structures. Each ply is usually rotated by a determined angle with respect to adjacent plies in order to improve the composite material strength. Examples of application include: speed brakes and rotor blades. Sandwich structures are another important category of composites. They consist of two stiff skins, typically metallic, plastic or composite having great

*Corresponding author. Email: maldagx@gel.ulaval.ca

Nondestructive Testing and Evaluation
ISSN 1058-9759 print/ISSN 1477-2671 online © 2007 Taylor & Francis
http://www.tandf.co.uk/journals
DOI: 10.1080/10589750701448548

mechanical strength, separated by a low-density material core spacer such as honeycomb or foam, providing better distribution of loading than a simple laminate (Marinetti *et al.* 2000). Many aircraft parts are now produced using sandwich structures: ailerons, flaps, keels, rudders, etc. (Vavilov *et al.* 2003).

The integrity of composite components can be impaired in several ways. During the fabrication stages, subsurface flaws such as voids, delaminations, inclusions, porosity and regions having unbalanced fiber content, may result from inadequate production procedures. Subsequent machining, e.g. drilling or cutting, may produce cracks and delaminations if improperly executed. Aerospace parts can be affected during normal operation as well. For instance, impact of hard bodies, e.g. birds or artillery, may damage (e.g. fiber breakage) the fuselage and other exposed surfaces, or atmosphere water can penetrate the core due to possible imperfections in joints (Marinetti *et al.* 2000, Crane *et al.* 2001).

Visual inspection and tap-test have been traditionally used in aerospace NDT&E. However, the industry is gradually moving towards qualitative and quantitative techniques relying to a lesser extent on the skills and training of an operator. At present, several NDT&E techniques are used in aerospace applications (Taylor and Dupont 1998, Marinetti *et al.* 2000): optical testing (shearography, holography), radiographic inspection (neutron radiography, X-rays), eddy current, thermal methods (thermography) and ultrasonic testing, with the latter being perhaps the most commonly used inspection technique for aerospace components. In conventional ultrasonic testing, the transducer must be maintained normal to the inspected part during the acquisition (Taylor and Dupont 1998), which is relatively easy to perform on small flat parts but become more complicated during inspection of large non-planar and large surfaces. Further complications are related to the high degree of automation and advanced data processing that are required (Achenbach 2000). Infrared (IR) thermography is gaining in popularity thanks to its rapid inspection and high portability of detection. For instance, trapped water at cruising flight height becomes frozen and remains cold for long time (2–3 h) after landing, which allows to *passively*, i.e. without using any external source of energy, detect water. In contrast, quantitative evaluation is difficult to perform on such a scheme. Ultrasounds on the contrary would have no problem on assessing the water content by determining the height of a water column in a cell for example (Vavilov *et al.* 2003). However, it could take a long time to identify the regions with water ingress in a point-to-point technique and the inspected part has to be moved to the ultrasound laboratory. An interesting approach is to combine both techniques: thermography can be used for the initial detection and ultrasounds for subsequent characterization (Achenbach 2000).

On the other hand, *active* thermography, i.e. using an external energy source, can be considered as a completely autonomous technique, competing in some cases with ultrasound in terms of accuracy of detection (Taylor and Dupont 1998). Besides, in some cases, active thermography might be the most suitable technique to perform the inspection, e.g. when only one side of the specimen is available and for detecting corrosion around rivets (Maldague 2001). Furthermore, as noted by (Burleigh 1999), active thermographic techniques present other advantages over ultrasonic testing: it is less time consuming, less expensive, portable (no need to move the inspected parts to the lab), subsurface defects location can be marked on the surface, and there is no risk of water permeation during the inspection.

Pulsed thermography (PT) is an active technique in which, the thermal energy is delivered by means of optical devices e.g. photographic flashes to the surface, where the light is

transformed into heat. Thermal waves propagate by conduction through the specimen until they reach a discontinuity that act as a resistance reflecting the thermal waves back to the surface. PT is particularly interesting for the inspection of aerospace materials such as sandwich structures and composites given that, after submitting the specimen surface to a thermal front, the most common types of subsurface discontinuities can be detected with an IR camera as regions showing abnormal temperature patterns.

In this paper, we present the basic experimental configuration for PT; we review three advanced signal processing techniques and illustrate their applications through some examples. We begin our discussion by describing the data acquisition system used in PT.

2. Data acquisition

Data acquisition by PT is fast and straightforward as illustrated in figure 1. The specimen surface is submitted to a heat pulse (2–15 ms) using a high power source such as photographic flashes. After the thermal front came into contact with the specimen's surface, the thermal waves travel from the surface through the specimen. As time elapses, the surface temperature will decrease *uniformly* for a piece without internal flaws. On the contrary, subsurface discontinuities can be thought as resistances to heat flow that produce abnormal temperature patterns at the surface, which can be recorded with an IR camera. A synchronization unit is needed to control the time between the launch of the thermal pulse and the recording. Data is stored as a 3D matrix as depicted in figure 2a, where x and y are the spatial coordinates, and t is the time. The temperature of a point on the surface decreases at a rate that can be approximated by the square root of time ($t^{1/2}$), at least at early times, as predicted by equation (3) except for the defective areas, where the cooling rate is different as seen in figure 2b.

The first parameters that need to be determined in any PT experience are the frame rate f_s, and the acquisition time t_{acq}. These two parameters are intimately related and are limited by the maximum storage capacity of the IR system: $N_{max} = f_s t_{acq}$. Appropriate selection of f_s and t_{acq} primarily depends on the thermal properties of the specimen. In general, high

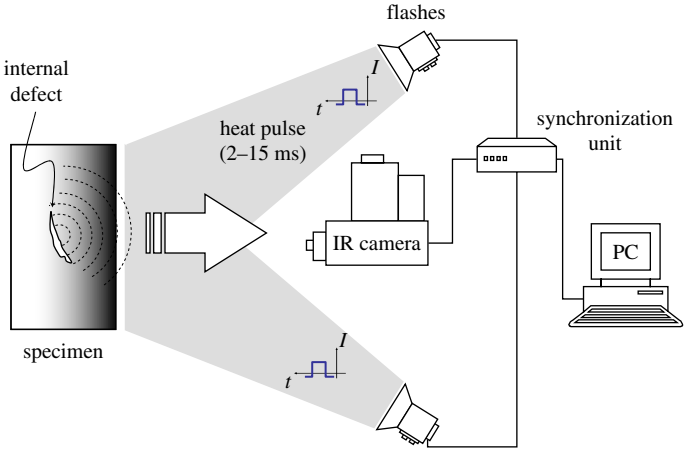

Figure 1. Data acquisition by PT.

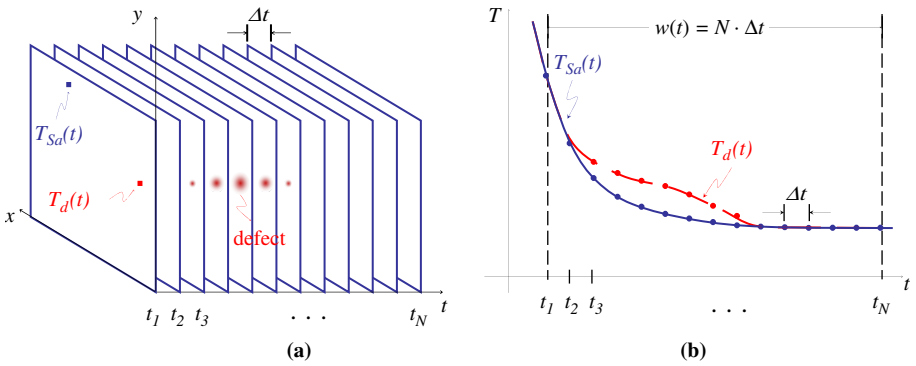

Figure 2. Thermal data: (a) 3D matrix, (b) thermal profile for a pixel (i,j).

conductivity materials require a faster f_s (to avoid loss of information), but shorter t_{acq} (given that thermal variations ends more rapidly) than poor thermal conductors.

During the acquisition process, the continuous temperature signal $T(t)$, is sampled at a given temporal resolution Δt, and truncated with a rectangular window $w(t)$, as depicted in figure 2. The maximum time resolution corresponds to $\Delta t = 1/f_s$, (where f_s is the frame rate) and the maximum window size is $w(t) = t_{\text{acq}}$. The total number of recorded thermograms N, results from the combination of the two acquisition parameters: $N = w(t)/\Delta t$.

PT basic theory is addressed next.

3. Basic theory

Heat diffusion through a solid is a complex 3D problem that can be described by the Fourier's law of heat diffusion or the *heat equation* (Carslaw and Jaeger 1959):

$$\nabla^2 T - \frac{1}{\alpha}\frac{\partial T}{\partial t} = 0 \tag{1}$$

where ∇ is the 3D del operator, $\alpha = k/\rho c_P$ [m^2/s] is the thermal diffusivity of the material being inspected, k [W/mK] its thermal conductivity, ρ [kg/m^3] its density and c_P [J/kg K] its specific heat at constant pressure.

The 1D solution of the Fourier equation for the propagation of a *Dirac* heat pulse, i.e. an ideal waveform defined as an intense unit-area pulse of so brief duration that no measuring equipment is capable of distinguishing it from even shorter pulses (Bracewell 1965), in a semi-infinite isotropic solid by conduction has the form (Carslaw and Jaeger 1959):

$$T(z,t) = T_0 + \frac{Q}{\sqrt{k\rho c_P \pi t}} \exp\left(-\frac{z^2}{4\alpha t}\right) \tag{2}$$

where Q [J/m^2] is the energy absorbed by the surface and T_0 [K] is the initial temperature.

A Dirac heat pulse is composed of periodic waves at *all* frequencies and amplitudes. It is not possible to reproduce such a waveform in practice, as a heat pulse provided by a powerful source such as a photographic flash, has *approximately* a square shape (see Maldague *et al.* 2004 for a discussion on this). In this case, the signal is composed of periodic waves at *several* (but not all) frequencies. The shorter the pulse, the broader is the range of frequencies

it contains. At the surface ($z = 0$ mm), equation (2) can be rewritten as follows:

$$T(0,t) = T_0 + \frac{Q}{e\sqrt{\pi t}} \tag{3}$$

where $e = (k\rho c_P)^{1/2}$ $[m]$ is the effusivity, which is a thermal property that measures the material ability to exchange heat with its surroundings.

Although equation (3) is only an approximation of the complex 3D diffusion problem described by Fourier's law, i.e. equation (1), many of the PT processing techniques have been based on this simplification to perform qualitative and quantitative analysis. The next section presents two of such techniques that rely on equation (3), and a third one based on the Fourier transformed space to analyse PT data. These techniques are considered to be some of the most promising among many others and they are currently subject to extensive research.

4. Processing

PT is probably the most extensively investigated active thermal approach because of its ease of deployment. Raw PT data however, is often difficult to handle and analyse. There are a great variety of processing techniques that have been developed to enhance the subtle IR signatures (Maldague 2001, Ibarra-Castanedo *et al.* 2004a, 2005a). Space being limited, it is only possible to discuss a few of them in this paper. We selected three techniques that have shown very promising results for most common applications. Although only a brief discussion is provided; interested readers may consult the references provided.

4.1 Differentiated absolute contrast, DAC

Thermal contrast is a basic operation that despite its simplicity is at the origin of many PT algorithms. Various thermal contrast definitions exist (Maldague 2001, p. 198), but they all share the need for specifying a sound area Sa, i.e. a non-defective region. For instance, the *absolute* thermal contrast $\Delta T(t)$ is defined as (Maldague 2001):

$$\Delta T(t) = T_d(t) - T_{\mathrm{Sa}}(t) \tag{4}$$

with $T_d(t)$ the temperature of a pixel or the average value of a group of pixels on a defective area at time t, and $T_{\mathrm{Sa}}(t)$ the temperature at time t for the Sa. No defect can be detected at a particular t if $\Delta T(t) = 0$. In practice however, raw data is contaminated with noise and other signal degradations (Maldague 2001, p. 105, 181), and a threshold of detectability needs to be established.

The main drawback of classical thermal contrast is establishing Sa, especially if automated analysis is needed. Even when Sa definition is straightforward, considerable variations on the results are observed when changing the location of Sa (Martin *et al.* 2003).

In the differential absolute contrast (DAC) method (Pilla 2002, Pilla *et al.* 2002), instead of looking for a non-defective area, an *ideal* Sa temperature at time t is computed locally assuming that on the first few images (at least one image at time t' in particular) this local point behaves as a Sa in accordance to equation (3), i.e. there is no visible defect. The first step is to define t' as a given time value between the instant when the pulse has been launched, and the precise moment when the first defective spot appears on the thermogram

sequence, i.e. when there is enough contrast for the defect to be detected. At t', there is no indication of the existence of a defect yet, therefore, the local temperature for a Sa is exactly the same as for a defective area (Pilla 2002):

$$T_{\mathrm{Sa}}(t') = T(t') = \frac{Q}{e\sqrt{\pi t'}} \Rightarrow \frac{Q}{e} = \sqrt{\pi t'}T(t') \tag{5}$$

From this result, T_{Sa} can be computed for every pixel at time t. Substituting equation (5) into the absolute contrast definition, i.e. equation (4), it follows that (Pilla 2002):

$$\Delta T_{\mathrm{DAC}} = T_d(t) - \sqrt{\frac{t'}{t}}T(t') \tag{6}$$

Actual measurements diverge from the solution provided by equation (6) as time elapses and also as the plate thickness increases with respect to the non-semi-infinite case. Nevertheless, the DAC technique has proven to be very efficient by reducing artefacts from non-uniform heating and surface geometry and providing a good approximation even for the case of anisotropic materials at early times (Ibarra-Castanedo *et al.* 2005a). Originally, proper selection of t' required an iterative graphical procedure, for which a graphical user interface was developed (Klein *et al.* 2007). An automated algorithm is also available (González *et al.* 2004). Furthermore, a modified DAC technique based on a finite plate model and the thermal quadrupoles theory has been developed as well (Benítez *et al.* in press a). The solution includes the plate thickness L explicitly in the solution, extending in this way the validity of the DAC algorithm to later times. Finally, the DAC algorithm has also been proposed to be used in combination with pulsed phase thermography (PPT) data (see section 4.3), to eliminate the need for manual definition of a reference area and provide an automated tool for the determination of the depth of subsurface defects.

4.2 Thermographic signal reconstruction, TSR

Thermographic signal reconstruction (TSR) (Shepard 2001, Shepard *et al.* 2002) is an attractive technique that allows increasing spatial and temporal resolution of a sequence, while reducing at the same time the amount of data to be manipulated. TSR is based on the assumption that temperature profiles for non-defective pixels should follow the decay curve given by the one-dimensional solution of the Fourier equation, i.e. equation (3), which may be rewritten in the logarithmic form as:

$$\ln(\Delta T) = \ln\left(\frac{Q}{e}\right) - \frac{1}{2}\ln(\pi t) \tag{7}$$

As stated before, equation (3) is only an approximation of the solution for the Fourier equation. To fit the thermographic data, Shepard 2001 proposed to use a p-degree polynomial of the form:

$$\ln(\Delta T) = a_0 + a_1 \ln(t) + a_2 \ln^2(t) + \cdots + a_p \ln^p(t) \tag{8}$$

Thermal profiles corresponding to non-defective areas in the sample will follow an approximately linear decay, while the thermal behaviour of a defective area will diverge from linearity. Typically, p is set to 4 or 5 to avoid "ringing" and insure a good correspondence between acquired data and fitted values. At the end, the entire raw thermogram sequence

is reduced to $p + 1$ coefficient images (one per polynomial coefficient) from which *synthetic* thermograms can be reconstructed.

Synthetic data processing brings interesting advantages such as: significant noise reduction, possibility for analytical computations and data compression (from N to $p + 1$ images). Analytical processing also becomes possible, giving the possibility of estimating the *actual* temperature for a time between acquisitions from the polynomial coefficients. Furthermore, calculation of first and second time derivatives from the synthetic coefficients is straightforward. First time derivatives indicate the rate of cooling while second time derivatives refer to the rate of change in the rate of cooling. Therefore, time derivatives are more sensitive to temperature changes than raw thermal images. There is no purpose using higher order derivatives, since, besides the lack of a physical interpretation, no defect contrast improvement can be observed. Finally, TSR synthetic data can be used in combination with other algorithms to perform quantitative analysis as described at the end of the next section.

4.3 Pulsed phase thermography, PPT

PPT (Maldague and Marinetti 1996, Maldague and Couturier 1997, Ibarra-Castanedo and Maldague 2004) is another interesting technique, in which data is transformed from the time domain to the frequency domain using the one-dimensional discrete Fourier transform (DFT) (Bracewell 1965):

$$F_n = \Delta t \sum_{k=0}^{N-1} T(k\Delta t) \exp^{(-j2\pi mk/N)} = \mathrm{Re}_n + j\,\mathrm{Im}_n \tag{9}$$

where j is the imaginary number ($j^2 = -1$), n designates the frequency increment ($n = 0,1,\ldots N$), Δt is the sampling interval, and Re and Im are the real and the imaginary parts of the transform, respectively.

In this case, real and imaginary parts of the complex transform are used to estimate the amplitude A, and the phase ϕ (Maldague and Marinetti 1996):

$$A_n = \sqrt{\mathrm{Re}_n^2 + \mathrm{Im}_n^2} \tag{10}$$

$$\phi_n = \tan^{-1}\left(\frac{\mathrm{Im}_n}{\mathrm{Re}_n}\right) \tag{11}$$

The DFT can be used with *any* waveform (e.g. transient pulsed thermographic profiles). Figure 3a portrays the 3D phase matrix reconstructed from pulsed data using equation (11). The phase profiles for a defective (red) and a non-defective (blue) pixels are shown in figure 3b. As can be seen in this figure, the phase profiles for this type of signal, i.e. decaying surface temperature, are anti-symmetric, providing redundant information in both sides of the frequency spectra. In the following, only the positive part of the frequency spectra is used whilst the negative frequencies can be safely discarded.

Although very useful, equation (9) is slow. Fortunately, the fast Fourier transform (FFT) algorithm is available (Cooley and Tukey 1965) to be implemented or can be found (integrally or simplified) in common software packages. The use of the DFT, or more precisely the FFT on thermographic data was first proposed by (Maldague and Marinetti

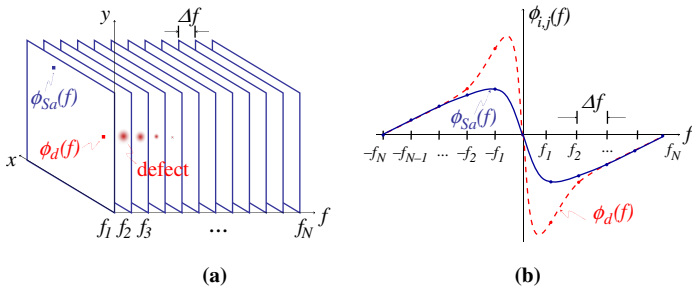

Figure 3. Phase data from PPT: (a) 3D matrix, (b) phase profile for a pixel (i,j).

1996). Since then, it has been applied to other thermographic data, such as lock-in and vibrothermography (Dillenz *et al.* 2001, 2002).

The phase is of particular interest in NDE given that it is less affected than raw thermal data by environmental reflections, emissivity variations, non-uniform heating and surface geometry and orientation. These phase characteristics are very attractive not only for qualitative inspections but also for quantitative characterization of materials. For instance, a depth inversion technique using the phase from PPT has been proposed (Ibarra-Castanedo 2005). The technique relies on the thermal diffusion length equation, i.e. $\mu = (\alpha/\pi \cdot f)^{\frac{1}{2}}$, in a manner similar to lock-in thermography (LT) (Meola and Carlomagno 2004). The depth of a defect can be calculated from a relationship of the form (Ibarra-Castanedo 2005):

$$z = C_1 \cdot \mu = C_1 \sqrt{\frac{\alpha}{\pi \cdot f_b}} \tag{12}$$

where f_b [Hz] is the blind frequency defined as the limiting frequency at which a defect located at a particular depth presents enough (phase or amplitude) contrast to be detected on the frequency spectra.

Defect contrast is enhanced using the phase (given the phase properties described above) allowing deeper probing. Conventional experimental C_1 values when using the phase from LT experiments range between 1.5 and more than 2 (Busse 1979), with a value of $C_1 = 1.82$ (Thomas *et al.* 1980) typically adopted in experimental studies (Meola and Carlomagno 2004). PPT results agree with these numbers for homogeneous materials (Ibarra-Castanedo 2005): $C_1 \sim 1.72$ for steel, and $C_1 \sim 2.0$ for Plexiglas®, and for composite materials (Ibarra-Castanedo and Maldague 2005): $C_1 \sim 1.73$ for CFRP. In this way, the inversion problem in PPT is reduced to the estimation of f_b from the phase.

Figure 4 illustrates the depth retrieval procedure using the phase contrast. The phase profiles for the positive part of the spectra for two defects at different depths (ϕz_1, ϕz_2), and for a sound area (ϕ_{Sa}), are shown at the bottom part of this graph. Phase contrast ($\Delta\phi z_1$, $\Delta\phi z_2$) can be calculated from the phase profiles as: $\Delta\phi = \phi_d - \phi_{\mathrm{Sa}}$, where ϕ_d is the phase of a defective pixel, and ϕ_{Sa} is the phase for a non-defective pixel. The negative value for the phase contrast is used for convenience. Defects are visible (i.e. $\Delta\phi > 0$) from $f = 0$ Hz to the blind frequency f_b, which is lower for deeper defects ($f_b{,}z_1 > f_b{,}z_2$). Phase profiles for defective pixels merge with the phase profile for a sound area into a straight line for frequencies higher than the corresponding blind frequencies ($f > f_b$). Consequently, shallow defects have a larger frequency range of visibility than deep ones. The phase contrast has been proposed to determine f_b, but automatic determination of f_b without the need of a sound area definition is also possible (Ibarra-Castanedo *et al.* 2004b).

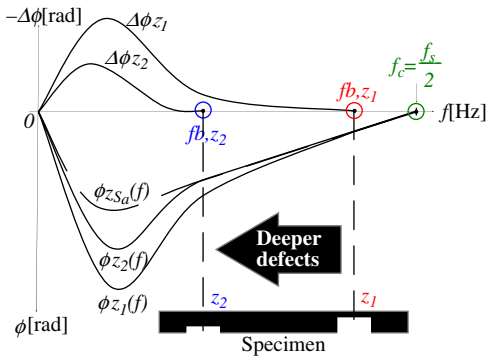

Figure 4. Depth retrieval from the PPT phase for the case of thick defects.

As with any other thermographic technique, PPT is not without drawbacks. It is well-known that noise content present in phase data is considerable, especially at high frequencies. This causes a problem for the determination of the blind frequency. A de-noising step is therefore often required. The combination of PPT and TSR has proven to be very effective for this matter, reducing noise and allowing the depth retrieval for a defect (Ibarra-Castanedo *et al.* 2005b). An example is shown below. Another difficulty is that, given the time–frequency duality of the Fourier transform, special care must be given to the selection of the sampling and truncation parameters prior to the application of the PPT. These two parameters depend on the thermal properties of the material and on the depth of the defect, which are often unknown. An interactive procedure has been proposed for this matter (Ibarra-Castanedo and Maldague 2005). The importance of the sampling and truncation parameters will be highlighted in one of the examples presented below.

As a final note, the FFT is typically used to extract amplitude and phase information in PPT. Nevertheless, it is also possible to use different transformation algorithms such as wavelet transforms (Galmiche *et al.* 2000, Zauner *et al.* 2006). The latter has the additional advantages of preserving the temporal information after the transformation and to use *wavelets* as the basis function instead of sinusoids. Wavelets are periodic waves of short duration that allow a better reproduction of a transient signal and usage of different scales or resolutions (Ibarra-Castanedo *et al.* in press). These advantages of the wavelet transform are currently under investigation.

The next section presents two examples of the described processing techniques. More results are available in the references provided all through the paper.

5. Results

5.1 Experimental setup

The experimental configuration is depicted in figure 1. Acquisition was carried out using an IR camera (ThermaCAM® Phoenix® from FLIR Systems,14 bits, InSb 640 × 512 FPA, 3–5 μm, Stirling closed cycle cooler), working at a sampling frequency of 87.8 Hz. Two high power flashes (Balcar FX 60), giving 6.4 kJ for 2 ms each, were used as heating sources. Thermographic data was analysed with a PC (Pentium® 4, 2 GB RAM) using MATLAB® environment from The MathWorks, Inc.

5.2 Honeycomb aircraft door

Figure 5 shows a GFRP door with a honeycomb core developed for Airbus by SABCA Limburg N. V. (Société Anonime Belge de Constructions Aéronautiques). Photographs displaying the front and rear views are shown in figure 5a,b, respectively. The front view photograph exhibits four distinctive repair zones at the surface. The rear view photograph on the contrary shows no repairs but two spots that reveal an inserted material used to simulate water ingress. Figure 5c and d display two zoomed portions (black dotted rectangles in figure 5a,b, respectively) of the door with enhanced contrast to provide more details about two features of interest (see discussion below). The specimen's front surface was painted in black, as seen in figure 5e, and inspected by PT. An early raw thermogram ($t = 12.5$ ms) is shown in figure 5f.

It is possible to detect all four repair zones and other surface features such as adhesive tape, adhesive tape residues and brush trail marks (left during the application of water-based black painting) from the raw thermal data in figure 5f. Processing results however, reveal more surface and subsurface details. For instance, figure 6a presents the DAC results for early

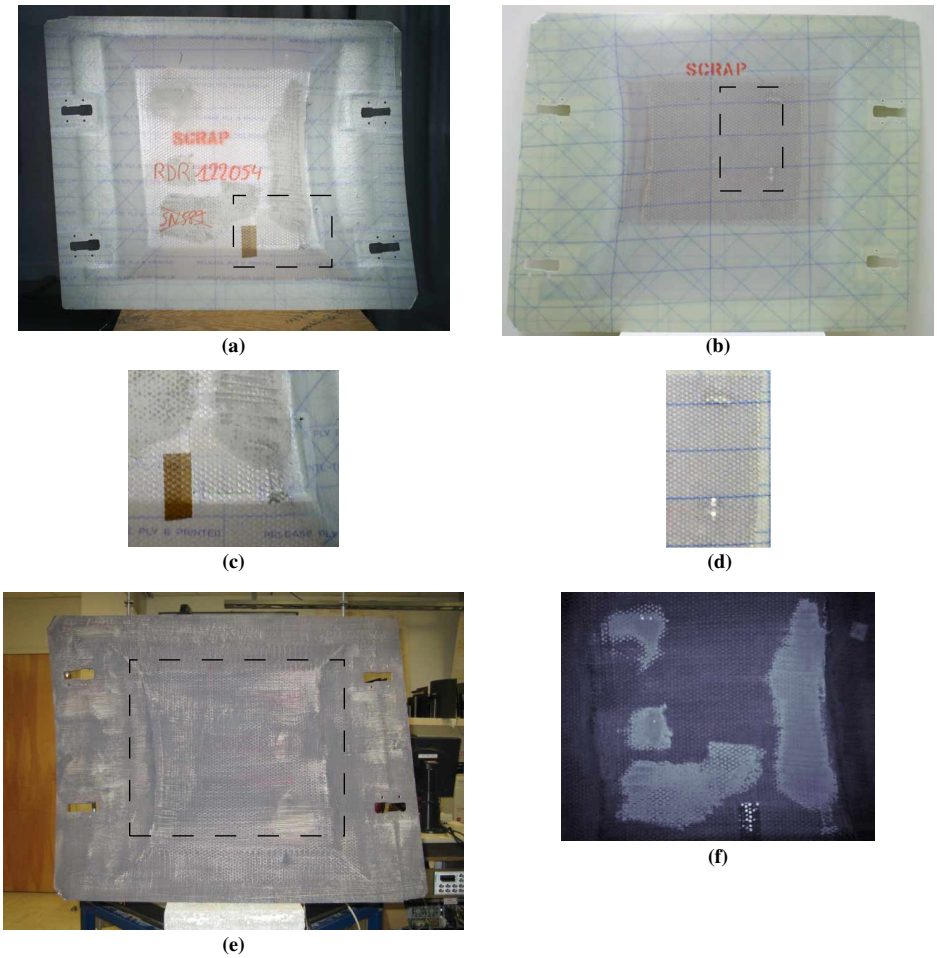

Figure 5. Airbus door specimen: (a) front and (b) back sides of the panel without blackpainting the surface, (c) front side with surface painted in black, and (d) raw thermogram at $t = 12.5$ ms after the flash.

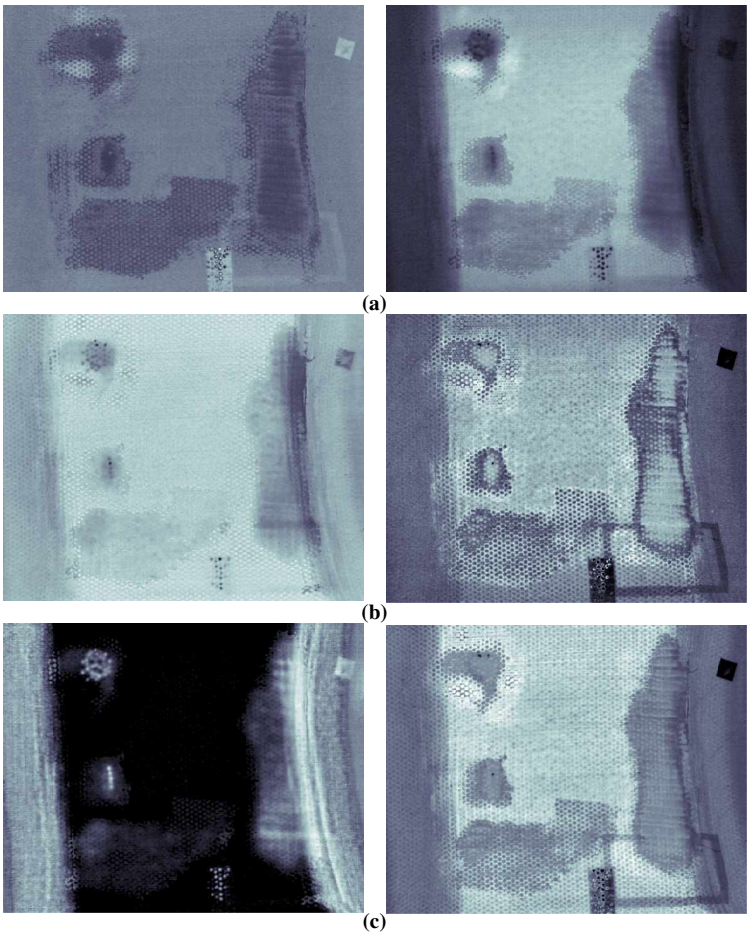

Figure 6. Comparative qualitative results for an Airbus door specimen. Processing results (a) DAC results at $t = 12.5$ ms (left) and $t = 4.5$ s (right); (b) TSR results for a 7th degree polynomial fitting: time derivative at $t = 1.25$ s (left) and second time derivative (right) at $t = 0.16$ s; and (c) PPT phase at $f = 0.04$ Hz (left) and $f = 0.45$ Hz (right).

($t = 12.5$ ms, left) and later ($t = 4.5$ s, right) times. The early time result (figure 6a, left) shows the same features as the raw thermogram, but the impact of the surface shape, painting and marks, as well as non-uniform heating is less significant due to the local contrast calculations. This allows detection of a square mark, which can also be inferred from figure 5c, but that is not seen in the raw thermogram corresponding to the same instant (see figure 5f). Later DAC results (figure 6a, right) uncover deeper features, i.e. the water ingress simulated defects seen from the back side of the panel in figure 5d.

First and second time derivatives obtained by TSR are presented in figure 6b. These images were manually picked from the entire sequence as the ones presenting the *best* contrast (qualitatively). The first time derivative result was selected as the one showing the best contrast for the water ingress defects, while the second derivative results exhibit the square mark with very good contrast.

Finally, figure 6c presents the PPT phase results at two frequencies. On the left, a very low frequency ($f = 0.04$ Hz) allows detection of deep characteristics (water ingress); whilst

on the right, at higher frequencies ($f = 0.45$ Hz), it is possible to see features that are at or very near the surface.

This example demonstrates the capabilities of the three techniques (DAC, TSR and PPT) for *qualitatively* detecting and analysing surface and subsurface defects in aerospace components. However, it is also important to carry out *quantitative* analysis in many cases. The next paragraph explains how TSR and PPT can be combined to estimate the depth of internal defects. An example of a combination of the DAC technique with PPT is available in (Benítez *et al.* in press b).

5.3 Rudder specimen

Flight control surfaces of F-18 aircraft, such as rudders, are another example of aerospace structure made of honeycomb sandwich material. Front (left) and rear (right) side photographs of the rudder used for the PT experiments are shown in figure 7. Figure 8 presents the phasegrams at three frequencies for the case of PPT applied to raw thermograms (top) and to synthetic data obtained by TSR. The de-noising effect of the polynomial fitting is evident when comparing raw (top) and synthetic (bottom) results at 0.039 and 1.2 Hz, figure 8b,c, respectively.

Phase results obtained by PPT at different frequencies are shown in figure 9 for the front (left) and back (right) sides of the specimen. Two defective zones, highlighted with 2 dotted circles in figure 9c, were spotted when inspecting the piece from both the front and back sides. The defect contrast is better at low frequencies ($f = 0.02$ and 0.04 Hz in figure 9b,c, respectively), up to a frequency at which no internal defect can be detected ($f = 0.2$ Hz, figure 9d). When inspecting the specimen from the back side, 8 honeycomb cells were completely filled with water (injecting the fluid from the front side and inspecting the piece in reflection from the back side). Six of the seven cells were detected as seen in figure 9b (black dotted ellipse), only the second cell from the left is not visible at this frequency. Water in all seven cells is however detected at a higher frequency (figure 9c). There was probably less water in this particular cell, although no evident difference in water content, cell damage or foreign material inclusion was detected after visually examining the specimen after the experiment. The origin of the bright spot above the water filled cells (black dotted square in figure 9c, right) is unknown. Previous experiments without water ingress did not show any sign of it. It could be due to accidentally dropping water on the back surface, or it is possible that water migrated somehow from the cells below during the preparation of the specimen.

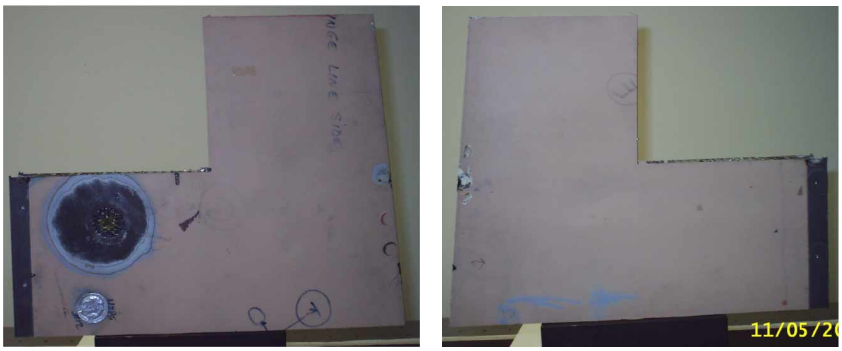

Figure 7. Rudder specimen: (a) front and (b) back side photographs.

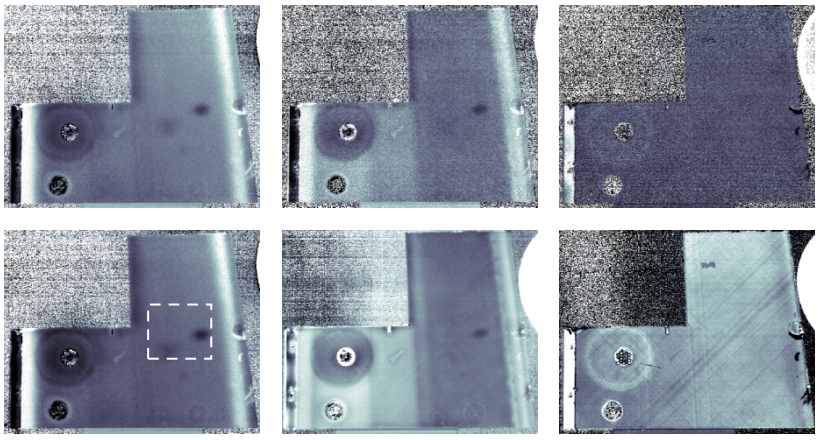

(a) **(b)** **(c)**

Figure 8. De-noising of the phase by applying the PPT algorithm to synthetic data by TSR: raw (top) and synthetic (bottom) PPT phase at $f =$ (a) 0.015, (b) 0.039 and (c) 1.2 Hz.

The next result demonstrates the need for careful selection of the acquisition and truncation parameters in PPT. Phasegrams in figure 10 were obtained by inspecting the specimen using two different conditions and applying the PPT algorithm to a region of interest (ROI) enclosing the two defects highlighted with a dotted square in figure 8a

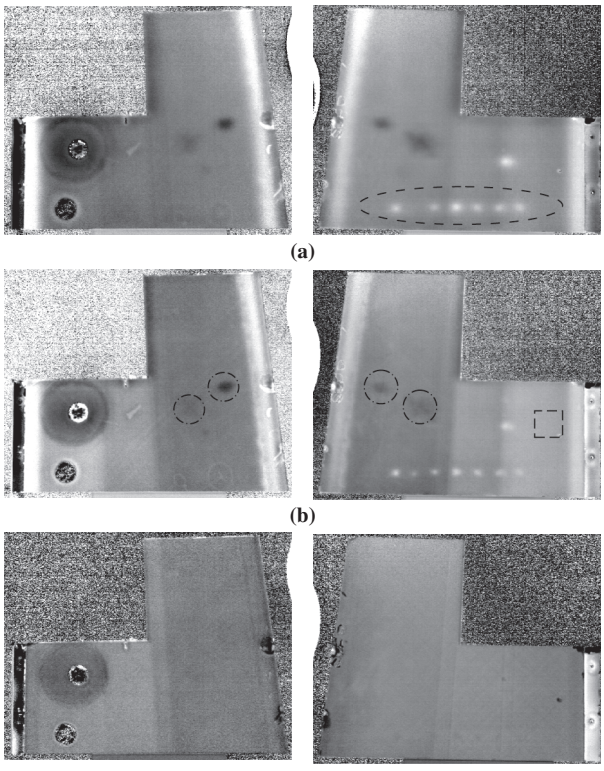

(a)

(b)

(c)

Figure 9. Rudder specimen: (a) front (left column) and back (right column) side photographs, and synthetic corresponding phasegrams (from a 9th degree TSR polynomial fitting) at $f =$ (b) 0.02, (c) 0.04, and (d) 0.2 Hz ($\Delta t = 860$ ms, $w(t) = 129$ s, $N = 150$).

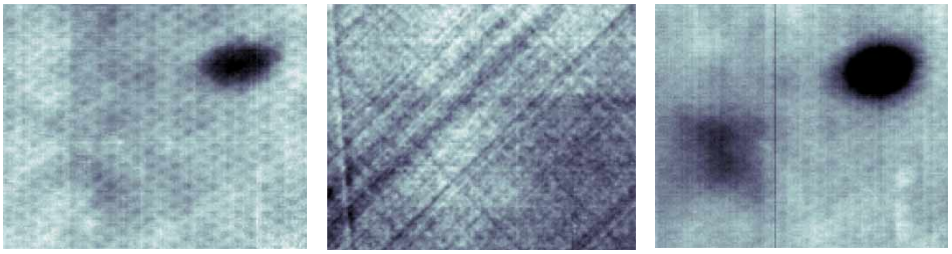

Figure 10. Synthetic PPT phasegrams (from a 5th degree TSR polynomial fitting) from the cropped area of the rudder specimen in figure 8c at $f =$ (a) 0.04, (b) 1.2 and (c) 0.0055 Hz. Acquisition parameters for (a) and (b): $\Delta t = 11$ ms, $w(t) = 26$ s, $N = 2300$; and for (c): $\Delta t = 79$ ms, $w(t) = 182$ s, $N = 2298$.

(bottom). The first experiment was carried out at a high sampling rate, i.e. $f_s = 87.8$ Hz, which provides a very good spatial resolution. At this sampling frequency, the acquisition only last for several seconds, i.e. $w(t) = 26$ s, since the buffer capacity of the system under this configuration is limited to $N = 2300$ images. The honeycomb cells are visible at low frequencies (figure 10a), and the carbon fibre matrix can be seen at high frequencies (figure 10b). Nevertheless, the selected acquisition time was not long enough to detect the subsurface defect (lower circle in figure 8c, bottom). In a second experiment, a lower sampling rate was used ($f_s = 12.4$ Hz) to increase the experiment duration ($w(t) = 182$ s) without reducing the number of images ($N = 2298$ images), which allows to retrieve phase data at even lower frequencies as seen in figure 10c. Although the spatial resolution was worsened by slowing down the frame rate, the longer acquisition time allowed detecting the subsurface defect.

Finally, figure 11 shows the quantitative results for the rudder specimen. A phasegram showing the defective and reference (Sound area, Sa) areas is presented in figure 11b. Phase and phase contrast profiles are shown in figure 11c and d, respectively. Given the considerably high noise levels affecting phase data, PPT was applied to a synthetic sequence obtained by TSR in order to detect the blind frequency f_b. This has an effective filtering effect on thermal data, which as seen produces de-noised phase profiles. The data filtering effect of applying the PPT algorithm to TSR synthetic data becomes more evident when analysing the phase contrast profiles in figure 11d. The PPT phase from raw thermal data is also included in these graphs to provide an indication of the levels of noise. The calculated blind frequencies allowed determining the depth of both defects: $z_1 = 0.5$ mm and $z_2 = 2$ mm. From these results it can be concluded that, defect number 1 is more likely due to an impact damage in the CFRP plies, while defect number 2 is deeper, corresponding possibly to a honeycomb crashed core. These observations were corroborated by visual (human) inspection.

6. Conclusions and future work

PT is an NDT&E technique for which data acquisition is fast, safe and portable. We discussed three promising processing techniques from the numerous approaches available in the literature. These three techniques have shown to considerably reduce the impact of common thermographic problems: surface emissivity variations, environmental reflections, non-uniform heating and non-planar surface, which provide results with enhanced contrast. In addition, the DAC approach provides the possibility of calculating the thermal contrast

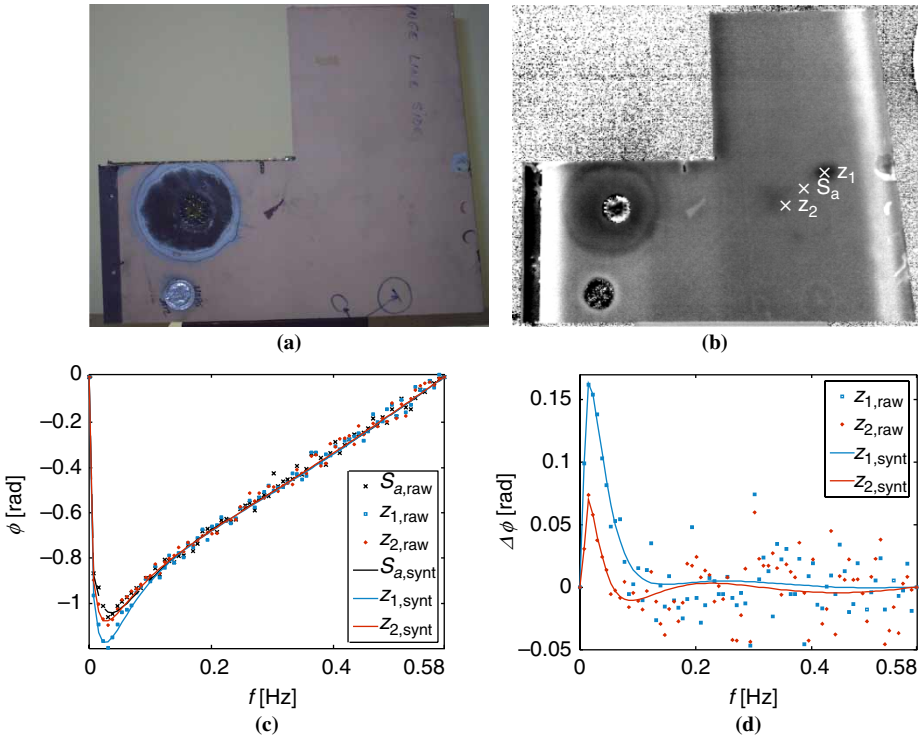

Figure 11. Quantification results using the synthetic phase from a 5th degree polynomial: (a) photograph of the rudder specimen, (b) phasegram showing the locations of the defects and the sound area, (c) phase and (d) phase contrast profiles for the areas identified in (a).

without defining a reference or sound area. TSR considerably reduces the amount of data to be handled and allow the arithmetic manipulation of data, which can be used to compute time derivatives or to retrieve temporal synthetic information between acquisitions. Moreover, a quantitative method for the estimation of the depth using PPT phase data is available.

The experimental results presented herein were intended to emphasize the capabilities of PT for qualitative and quantitative analysis of aerospace materials. Experience shows that there is no technique capable of perfectly solving all situations. On the contrary, we made an effort to expose the *pros* and *cons* of all three techniques presented in this paper. For instance, PPT allows *quantitatively* retrieving of deep information from the inspected sample, but the processed data (phase or amplitude) generally contains considerable amounts of noise, especially at high frequencies. This is very detrimental for the calculation of the blind frequency, the parameter used for extracting the defect depth. On the other hand, although no quantitative approach is available for TSR or DAC, these two approaches provide enhanced defect contrast and de-noised data. An interesting approach is to combine techniques in order to use the most attractive features from one technique and to reduce the non-desirable characteristics of the other. This *hybrid* approach has been described here for the quantification of subsurface defects in honeycomb structures, by applying the quantitative PPT approach to TSR de-noised and compressed data. Similarly, a DAC-PPT hybrid technique has been proposed elsewhere (Benítez *et al.* in press b), it combines the DAC de-noising and automated capabilities with quantitative PPT to automatically compute the depth of defects.

Research is now being directed to the development of qualitative and quantitative techniques for the inspection of new (and more demanding) aerospace materials such as Glare® and ceramics, towards the determination of the thickness of thin (delamination-like) defects, and to the investigation of signal transforms such as Hough, Radom, wavelets and Laplace for the analysis of the thermographic information in transformed spaces.

References

Achenbach, J.D., Quantitative nondestructive evaluation. *Int. J. Solids Struct.*, 2000, **37**, 13–27.

Benítez, H.D., Ibarra-Castanedo, C., Bendada, A., Maldague, X.P., Loaiza, H. and Caicedo, E., Definition of a new thermal contrast and pulse correction for defect quantification in pulsed thermography. *Infrared Phys. Technol.*, in press a.

Benítez, H.D., Ibarra-Castanedo, C., Bendada, A., Maldague, X.P., Loaiza, H. and Caicedo, E., Definition of a reference-free phase contrast for quantitative pulsed phase thermography. *NDT & E Int.*, in press b.

Bracewell, R., *The Fourier Transform and its Applications*, 1965 (McGraw-Hill: USA).

Burleigh, D., Thermograpic testing used on the x-33 space launch vehicle program by BFGoodrich aerospace. In *Proceedings SPIE—The International Society for Optical Engineering, Thermosense XXI*, edited by D.H. LeMieux and J.R. Snell, Jr, 3700, pp. 84–92, 1999 (Orlando: FL).

Busse, G., Optoacoustic phase angle measurement for probing a metal. *Appl. Phys. Lett.*, 1979, **35**, 759–760.

Carslaw, H.S. and Jaeger, J.C., *Conduction of Heat in Solids*, 1959 (Clarendon Press: Oxford).

Cooley, J.W. and Tukey, J.W., An algorithm for the machine calculation of complex Fourier series. *Math. Comput.*, 1965, **19**(90), 297–301.

Crane, R.L., Astarita, T., Berger, H., Cardone, G., Carlomagno, G.M., Jones, T.S., Lansing, M.D., Russell, S.S., Walker, J.L. and Workman, G.L., Chapter 15: Aerospace applications of infrared ans thermal testing: Part 3. Pulsed thermal inspection of aging aircraft. In *Nondestructive Handbook, Infrared and Thermal Testing*, edited by X. Maldague technical ed. and P.O. Moore, Vol. 3, 3rd edn, 718 p., 2001 (ASNT Press: Columbus, Ohio).

Dillenz, A., Zweschper, T. and Busse, G., Progress in ultrasound phase thermography. In *Proceedings SPIE—The International Society for Optical Engineering, Thermosense XXVIII*, edited by A.E. Rozlosnik and R.B. Dinwiddie, 4360, pp. 574–579, 2001 (Orlando: FL).

Dillenz, A., Zweschper, T. and Busse, G., Burst phase angle thermography with elastic waves. In *Proceedings SPIE—The International Society for Optical Engineering, Thermosense XXIV*, edited by X.P. Maldague, A.E. Rozlosnik and R.B. Dinwiddie, 4710, pp. 572–577, 2002 (Orlando: FL).

Ducar, R.J., Pulsed thermographic inspection and application in commercial aircraft repair. In *Proceedings SPIE, Thermosense XXI*, edited by D.H. LeMieux and J.R. Snell, 3700, pp. 77–83, 1999.

Galmiche, F., Vallerand, S. and Maldague, X., Pulsed phase thermography with the wavelet transform. In *Review of Progress in Quantitative NDE*, edited by D.O. Thompson and D.E. Chimenti, 19A, pp. 609–615, 2000 (American Institute of Physics: New York).

González, D.A., Ibarra-Castanedo, C., Pilla, M., Klein, M., López-Higuera, J.M. and Maldague, X., Automatic interpolated differentiated absolute contrast algorithm for the analysis of pulsed thermographic sequence. *Proceedings 7th Conference on Quantitative InfraRed Thermography (QIRT)*, pp. H16.1–H16.6, 2004 (Rhode Saint Genèse: Belgium), July 5–8.

Ibarra-Castanedo, C., Quantitative subsurface defect evaluation by pulsed phase thermography: depth retrieval with the phase, Ph. D. thesis, Laval University, 2005 [accessible online: http://www.theses.ulaval.ca/2005/23016/23016.pdf].

Ibarra-Castanedo, C. and Maldague, X., Pulsed phase thermography reviewed. *QIRT J.*, 2004, **1**(1), 47–70.

Ibarra-Castanedo, C. and Maldague, X., Interactive methodology for optimised defect characterization by quantitative pulsed phase thermography. *Res. Nondestruct. Eval.*, 2005, **16**(4), 1–19.

Ibarra-Castanedo, C., González, D., Klein, M., Pilla, M., Vallerand, S. and Maldague, X., Infrared image processing and data analysis. *Infrared Phys. Technol.*, 2004a, **46**(1–2), 75–83.

Ibarra-Castanedo, C., González, D.A. and Maldague, X., Automatic algorithm for quantitative pulsed phase thermography calculations. *16th WCNDT—World Conference on Nondestructive Testing* [CD ROM], Montreal (Quebec), August 30–September 3, 2004b.

Ibarra-Castanedo, C., Bendada, A. and Maldague, X., Image and signal processing techniques in pulsed thermography. *GESTS Int'l Trans. Comput. Sci. Engr.*, 2005a, **22**(1), 89–100, November.

Ibarra-Castanedo, C., Avdelidis, N.P. and Maldague, X., Quantitative assessment of steel plates using pulsed phase thermography. *Mater. Eval.*, 2005b, **63**(11), 1128–1133.

Ibarra-Castanedo, C., González, D.A., Galmiche, F., Bendada, A. and Maldague, X., Chapter 5: on signal transforms applied to pulsed thermography. *Recent Res. Devel. Applied Phys.*, 2007, **9**, 101–127, in press.

Klein, M., Pilla, M. and Maldague, X., IR_View: a graphical user interface to process infrared images with MATLAB, Application and documentation available online at: http://irview.m-klein.com (accessed February 21st 2007).

Maldague, X.P.V., Theory and practice of infrared technology for nondestructive testing, John Wiley-Interscience 684 p., 2001.

Maldague, X. and Couturier, J-P., Review of pulse phase infrared thermography. *Proc. 4th International Workshop on Advanced Infrared Technology and Applications (AITA)*, Firenze, Italy, September 15–16, 1997, **53**(1), 271–286.

Maldague, X.P. and Marinetti, S., Pulse phase infrared thermography. *J. Appl. Phys.*, 1996, **79**(5), 2694–2698.

Maldague, X., Ziadi, A. and Klein, M., Double pulse infrared thermography. *NDT & E Int.*, 2004, **37**, 559–564.

Marinetti, S., Muscio, A., Bison, P.G. and Grinzato, E., Modeling of thermal non-destructive evaluation techniques for composite materials. In *Proceedings SPIE, Thermosense XXII*, edited by R.B. Dinwiddie and D.H. LeMieux, 4020, pp. 164–173, 2000.

Martin, R.E., Gyekenyesi, A.L. and Shepard, S.M., Interpreting the results of pulsed thermography data. *Mater. Eval.*, 2003, **61**(5), 611–616.

Meola, C. and Carlomagno, G.M., Recent advances in the use of infrared thermography. *Meas. Sci. Technol.*, 2004, **15**, 27–58.

Pilla, M., A novel contrast method for pulse thermography data, Ph.D. Thesis, Politecnico di Milano, 2002.

Pilla, M., Klein, M., Maldague, X. and Salerno, A., New absolute contrast for pulsed thermography. In *Proceedings of QIRT*, QIRT 2002, edited by D. Balageas, G. Busse and G. Carlomagno, pp. 53–58, 2002.

Shepard, S.M., Advances in pulsed thermography. In *Proceedings SPIE—The International Society for Optical Engineering, Thermosense XXVIII*, edited by A.E. Rozlosnik and R.B. Dinwiddie, 4360, pp. 511–515, 2001 (Orlando: FL).

Shepard, S.M., Lhota, J.R., Rubadeux, B.A., Ahmed, T. and Wang, D., Enhancement and reconstruction of thermographic NDT data. In *Proceedings SPIE—The International Society for Optical Engineering, Thermosense XXIV*, edited by X.P. Maldague and A. Rozlosnik, 4710, pp. 531–535, 2002 (Orlando, FL).

Taylor, J.O. and Dupont, H.M., Inspection of metallic thermal protection systems for the X-33 launch vehicle using pulsed infrared thermography. In *Proceedings SPIE, Thermosense XX*, edited by J.R. Snell and R.N. Wurzbach, 3361, pp. 301–310, 1998.

Thomas, R.L., Pouch, J.J., Wong, Y.H., Favro, L.D. and Kuo, P.K., Subsurface flaw detection in metals by photoacustic microscopy. *J. Appl. Phys.*, 1980, **51**(2), 1152–1156.

Vavilov, V., Klimov, A., Nesteruk, D. and Shiryaev, V., Detecting water in aviation honeycomb structures by using transient IR thermographic NDT. In *Proceedings SPIE, Thermosense XXV*, edited by E. Cramer and X.P. Maldague, 5073, pp. 345–355, 2003.

Zauner, G., Mayr, G. and Hendorfer, G., Application of wavelet analysis in active thermography for nondestructive testing of CFRP composites. In *Proc. SPIE—The International Society for Optical Engineering, Wavelet Applications in Industrial Processing IV*, edited by F. Truchetet and O. Laligant, 6383, pp. 63830E1–63830E10, 2006.